ULTRA-WIDEBAND NON-RECIPROCAL MICRO-ACOUSTIC DELAY LINES WITH SLANTED-FINGER INTERDIGITAL TRANSDUCERS

Hakhamanesh Mansoorzare and Reza Abdolvand
University of Central Florida, USA

2022 IEEE 35th International Conference on Micro Electro Mechanical Systems Conference (MEMS) | 978-1-6654-0911-7/22/$31.00 ©2022 IEEE | DOI: 10.1109/MEMS51670.2022.9699654

ABSTRACT

Ultra-wideband (UWB) Lamb wave delay lines with non-reciprocal transmission are demonstrated in a suspended thin-film lithium niobate (LN)-on-silicon (Si) platform. Using slanted-finger interdigital transducers (SFIT) to efficiently excite fundamental symmetric (S_0) Lamb waves, up to 33% fractional bandwidth (6-dB) is realized at ~650 MHz. This is achieved through leveraging the strong interaction between drifting electrons in Si and piezoelectrically transduced acoustic waves – i.e. acoustoelectric (AE) effect – to compensate the problematic diffraction losses associated with SFIT and enable UWB non-reciprocal behavior. The non-reciprocity of the device is switched on and regulated by the bias applied along the device.

KEYWORDS

Acoustoelectric effect, Lamb waves, delay line, non-reciprocal, ultra-wideband.

INTRODUCTION

Acoustic waves provide a chip-scale solution for signal processing, owing to orders of magnitude slower wave velocity and lower loss compared to the electromagnetic waves. Consequently, today, surface acoustic wave (SAW) and bulk acoustic wave (BAW) components are widely present in frontend modules of wireless radios. Micro-acoustic delay lines providing sub-millimeter scale large real time delays, from few nanoseconds to microseconds depending on the phase velocity of the propagating mode, are finding applications such as filters, correlators, self-interference cancelers, to name a few. Acoustic modes guided in thin-films such as lithium niobate (LN) offer better confinement of electrical and acoustic energy therefore superior electromechanical coupling in comparison with SAW [1], [2]. Additionally, because of higher phase velocities and less sensitivity to surface imperfections relative to SAW, such acoustic modes can be efficiently excited at higher frequencies. In order to launch and detect the acoustic waves, interdigital transducers (IDT) are used with their periodicity determining the acoustic wavelength. By including a range of IDT periodicities rather that a single periodicity, a wider range of wavelengths could be supported, and the bandwidth of the device could become wider. In this category, slanted-finger interdigital transducers (SFIT) in which the periodicity of fingers changes along the aperture have enabled large bandwidths for SAW devices [3]. Such configuration can be regarded as multiple sub-channels with constant periodicity and narrow aperture in parallel with each other. This is conceptually illustrated in Figure 1. More recently, Lamb wave delay lines utilizing SFIT have been explored with an improved 6-dB below peak fractional bandwidth (FBW) of ~8% compared to conventional IDT designs [4]. However, the substantial diffraction losses associated with this type of transducers has resulted in a high IL (>26 dB) even for short delay lengths. Such losses occur because of the narrow aperture of each sub-channel and the fact that the room for increasing the total aperture is limited as the ohmic losses become significant, especially at high frequencies where the IDT width is very small.

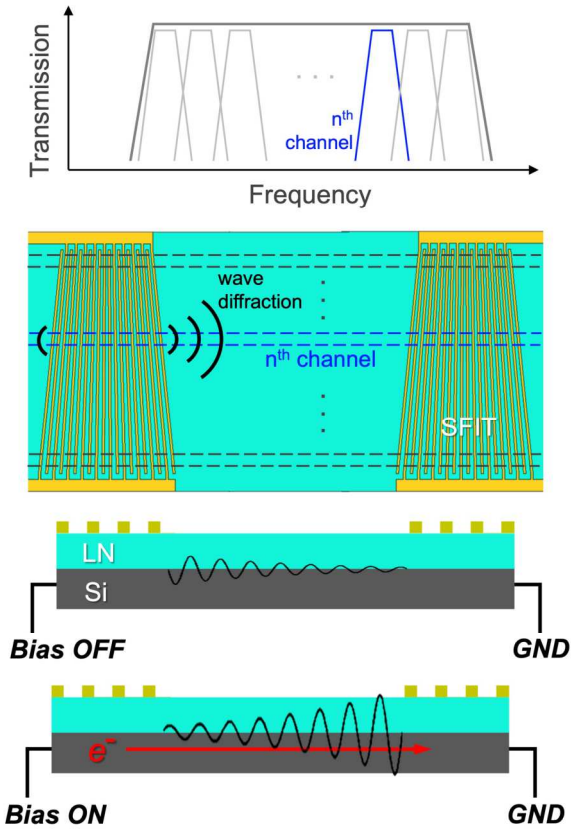

Figure 1: Conceptual schematic of SFIT where sub-channels with different pitch along the delay line aperture form a wide passband, AE gain and non-reciprocity is enabled by electrons drifting in Si underneath LN.

An attractive feature of the acoustic delay lines is the possibility of enforcing non-reciprocal transmission through the interactions between the acoustic waves and charge carriers, known as the acoustoelectric (AE) effect. Since the mid-twentieth century, amplification of BAW in piezoelectric semiconductors [5] and SAW in layered piezoelectric-semiconductor devices [6] have been observed. This is done by applying a large voltage so that the electrons drift faster than the acoustic waves and has enabled non-reciprocal transmission by amplifying the acoustic waves propagating in the direction of electrons

and attenuating the ones in the opposite direction. Although the recent advances in thin-film transfer and boding have allowed for AE SAW devices with better performance [7 - 9], the fundamental limitations of SAW are inevitable. Therefore, by switching to guided acoustic waves in thin film, stronger AE interactions and more efficient non-reciprocity could be realized at higher frequencies. Encouraged by the initial observation of AE effect in Lamb mode aluminum nitride (AlN) on silicon (Si) micro-acoustic devices [10], [11], we have previously reported power-efficient non-reciprocity in LN on Si Lamb mode delay lines [12]. Furthermore, by optimizing the thickness of Si in such structures, non-reciprocal transmission of larger than 30 dB was observed with only a few milliwatts of power consumption and under continuous operation [13]. In this work, based on the promising results obtained from AE effect in LN-Si S_0 mode delay lines, we aim to improve the non-reciprocal transmission bandwidth by taking advantage of SFIT. This way, the loss associated with this type of wideband transducers is compensated by the AE amplification and ultra-wideband (UWB) non-reciprocity is realized in an FBW of ~33%, defined as 6-dB below transmission peak.

DESIGN

The delay line is formed by an acoustically-thin stack of LN on Si with its length being defined by the two sets of SFIT and its width being defined by etching the stack. The device passband is tailored by the design of SFIT such as the finger pitch (FP) of the first and last sub-channel and the type of the transition between successive sub-channels. To further explain, the COMSOL simulated dispersion curve for S_0 mode in the LN-Si stack is shown in Figure 2; by choosing a FP of 6 µm for the lowest frequency and 4 µm for the highest frequency sub-channels, a frequency span of ~250 MHz is ideally expected to be covered by the SFIT. The scaling of FP from the lowest frequency to the highest frequency sub-channels can be linear or the FP of sub-channels can lean more towards the higher or lower frequency end as a mean of correcting the slope of the passband [14].

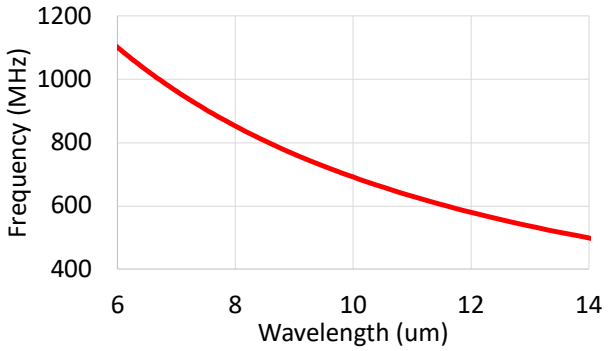

Figure 2: S_0 mode dispersion curve for the LN-Si stack showing ~250 MHz bandwidth covered by wavelengths from 8 µm to 12 µm.

Without applying a bias across the delay line, the device is reciprocal, yet a high insertion loss (IL) is expected, mainly due to the diffraction loss and AE loss. The diffraction loss occurs as the aperture, being the overlap between the fingers of opposite polarity, is too narrow and the launched waves deviate from the uniform planar wave approximation. This is shown in Figure 3 where the COMSOL simulated delay line displacement for three frequencies is illustrated, highlighting large diffraction, especially at input SFIT. AE losses occur as the acoustic phonons give up momentum to electrons in Si via the evanescent electric field in Si. Once the bias is applied and the electron drift velocity passes the threshold of S_0 mode phase velocity, the electrons start amplifying Lamb waves propagating along them and attenuate the ones propagating in their opposite direction. Therefore, the delay line becomes non-reciprocal based on the electron drift direction. The device presented in this work has a SFIT distance of 600 µm and width of 220 µm. The finger pitch linearly varies from 4 µm to 6 µm across the SFIT aperture and the LN-Si thicknesses are both ~1 µm. Two contact points to the Si layer are defined across the device length for the application of bias field for electron drift. The Si layer is lightly n-type doped to take advantage of its high electron mobility.

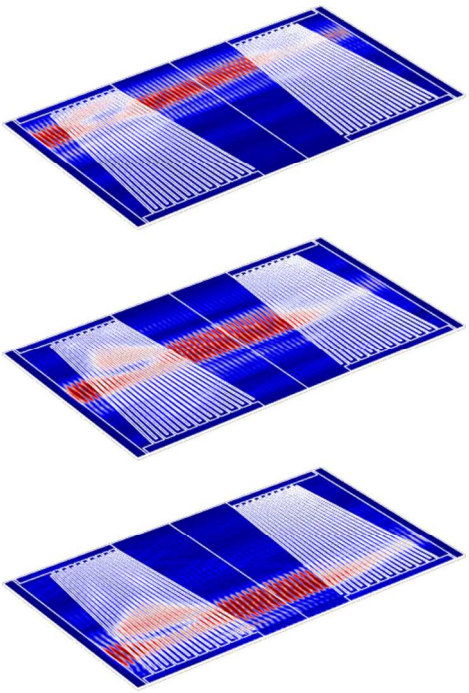

Figure 3: Displacement at a low, mid, and high passband frequency simulated by COMSOL. The excitation is from the left SFIT and the red color corresponds to maximum displacement.

FABRICATION

The delay lines are fabricated in a five-mask process. The X-cut LN wafer is rotated and bonded to an SOI wafer in a way that the 30º off +Y axis is aligned with the (110) Si plane. The bonded wafer is provided by NGK Insulators. Next, using e-beam evaporation and lift-off, a 25/75 nm Cr/Au is deposited and patterned to form the SFIT. The use of Cr is critical in enhancing the adhesion of SFIT to LN. The LN film is etched subsequently where the Si contact regions are designed, and such openings are overlayed with

Cr/Au (25/75 nm) for electrical contact. The lateral boundary of the delay lines is subsequently etched in an Ar-only RIE-ICP for the LN film followed by DRIE for the Si layer. This step also forms the current isolation trenches around the device to limit dissipated power. The backside of the wafer is etched next in DRIE to expose the buried oxide layer underneath the delay lines. The devices are finally released in buffered oxide etchant. These steps are summarized in Figure 4 and the scanning electron micrograph (SEM) of a typical device is shown in Figure 5.

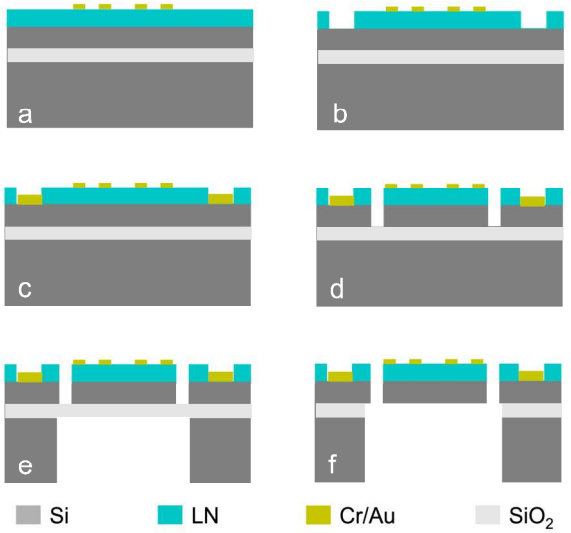

Figure 4: Summery of the fabrication process of the delay lines starting from the bonded LN-SOI wafer.

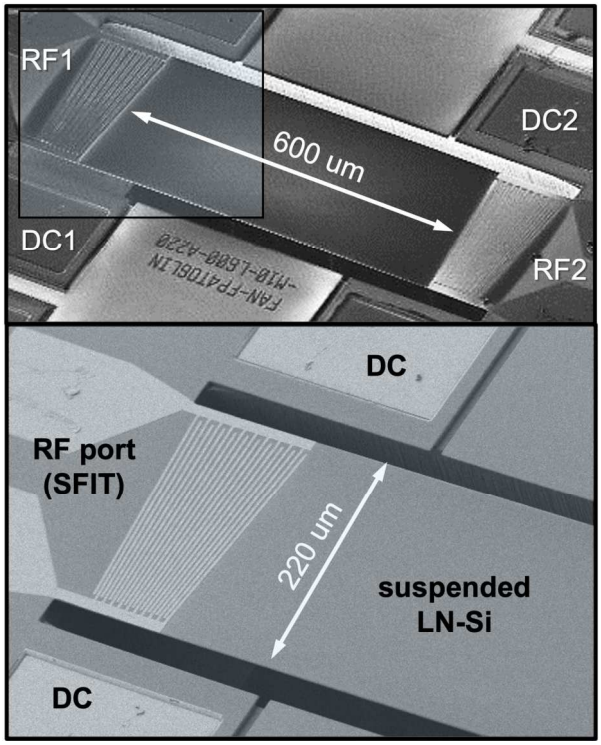

Figure 5: SEM of the UWB AE delay line having 600 µm separation between the two SFIT sets; the RF and DC contacts are marked, and the close-up shows the SFIT pattern with linearly varying FP of 4-6 µm

CHARACTERIZATION

The fabricated devices are characterized at room temperature and normal pressure using a Rohde & Schwarz ZNB8 network analyzer and calibrated GSG probes. The transmission (S_{21}) and reverse isolation (S_{12}) of a typical delay line with 600 µm mean distance between the two sets of SFIT is shown in Figure 6 with black and gray curves, respectively. This is prior to the bias application and due to the large diffraction and AE losses, the delay line is virtually off in its passband. Furthermore, the device is completely reciprocal as evident from the overlapping black and gray curves. Next, using a pair of DC microprobes, the drift voltage is applied to the Si contact points while the current passing through the body of delay line is measured by a current meter. As the bias voltage is increased so that the electron drift velocity reaches and exceeds the S_0 mode phase velocity, the transmission gradually improves, reaching a minimum IL of ~10.5 dB (plotted by the red curve) in Figure 6. In this case, the dissipated power is measured to be ~4.5 mW and the current meter shows 52 µA injected current. The measured 6-dB FBW is 33% while the minimum non-reciprocal transmission ratio is ~19 dB. From the blue curve, which shows the reverse isolation, large ripples due to the formation of standing waves between the two sets of SFIT are believed responsible for lowering the minimum non-reciprocal transmission ratio. From the red curve in Figure 6, a transmission dip is observed in the passband which is likely due to the destructive interference of sub-channels. This could be relieved by optimizing the SFIT design, for example through adjusting the phase of sub-channels via a stepped-SFIT configuration as suggested in [15].

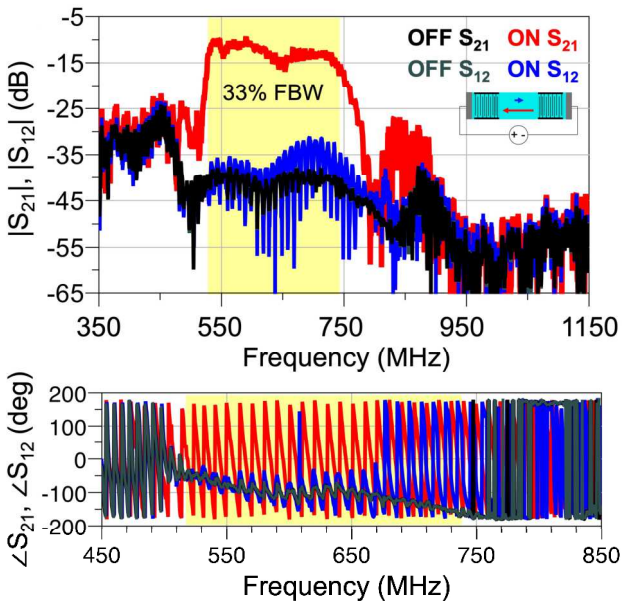

Figure 6: Measured wide-span magnitude and near-passband phase of transmission (S_{21}) and reverse isolation (S_{12}) of 600 µm delay line with SFIT before (black & gray) and after application of bias (red & blue); The measured dissipated bias power is 4.5 mW in this case.

The AE gain as a function of the bias voltage applied to the Si contacts across the delay line is shown in Figure

7. This is illustrated for a few frequencies within or close to the delay line passband. As expected, the frequencies within the passband experience a much larger AE gain.

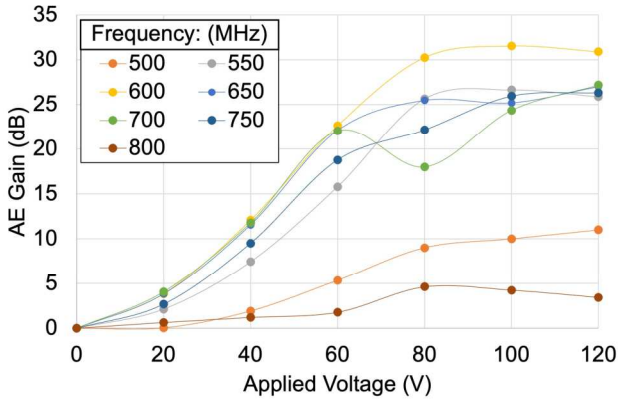

Figure 7: AE gain as a function of the applied voltage to Si contact points is plotted for a few frequency points close to the delay line passband.

CONCLUSIONS

The reported passband in the literature for SAW and Lamb mode AE delay lines have been so far limited to a few percent in fractional bandwidth (FBW). In this work, it was proposed and experimentally demonstrated that using slanted-finger interdigital transducers (SFIT) in an acoustically-thin lithium niobate (LN) on silicon (Si) Lamb wave delay line, FBW of up to 33% is attainable. Owing to the strong AE interactions between high electromechanical coupling S_0 mode and electrons in the Si layer, ultra-wideband (UWB) non-reciprocal transmission is realized and controlled by the bias voltage applied to the Si layer. The preliminary results present the highest FBW achieved in AE delay lines and further improvement of IL and elimination of spurs is expected by design optimizations in the future works.

ACKNOWLEDGEMENTS

This work was supported by the National Science Foundation (NSF) under Award 1810143.

REFERENCES

[1] R. Lu, and S. Gong. “RF acoustic microsystems based on suspended lithium niobate thin films: advances and outlook.” Journal of Micromechanics and Microengineering 31.11 (2021): 114001.

[2] M. Kadota, Y. Ishii, and S. Tanaka. “Ultra-wideband T- and π-type ladder filters using a fundamental shear horizontal mode plate wave in a LiNbO3 plate.” Japanese Journal of Applied Physics 58.SG (2019): SGGC10.

[3] T. Hyodo, K. Yamanouchi and K. Shibayama, “The wide band excitation of elastic surface waves using the interdigital electrodes with variable pitches”, Proc. Acoustic Society of Japan 1968 Autumn Annual Meeting 3-1-14, pp. 193-194, 1968-Nov.

[4] N. Kuo, J. S. Fernandez, and G. Piazza. “1 GHz bulk acoustic wave slanted finger interdigital transducers in aluminum nitride for wideband applications,” 2012 IEEE International Frequency Control Symposium Proceedings. IEEE, 2012.

[5] A. R. Hutson, J. H. McFee, and D. L. White. “Ultrasonic amplification in CdS.” Physical Review Letters 7.6, 1961.

[6] L. A. Coldren, and G. S. Kino. “Monolithic Acoustic Surface-Wave Amplifier.” Applied Physics Letters 18.8, 1971.

[7] S. Ghosh and M. Ricci, “A 3-Port Circulator Based on Non-Reciprocal Acoustoelectric Delay Lines,” 2020 Joint Conference of the IEEE International Frequency Control Symposium and International Symposium on Applications of Ferroelectrics (IFCS-ISAF), 2020, pp. 1-3.

[8] D. C. Malocha, C. Carmichael and A. Weeks, “Acoustoelectric Amplifier With 1.2-dB Insertion Gain Monolithic Graphene Construction and Continuous Wave Operation,” in IEEE Transactions on Ultrasonics, Ferroelectrics, and Frequency Control, vol. 67, no. 9, pp. 1960-1963, Sept. 2020.

[9] Hackett, Lisa, et al. “Towards single-chip radiofrequency signal processing via acoustoelectric electron–phonon interactions.” Nature communications 12.1 (2021): 1-11.

[10] H. Mansoorzare, R. Abdolvand and H. Fatemi, “Investigation of Phonon-Carrier Interactions in Silicon-Based MEMS Resonators,” 2018 IEEE International Frequency Control Symposium (IFCS), 2018, pp. 1-3.

[11] H. Mansoorzare and R. Abdolvand, “Acoustoelectric Amplification in Lateral-Extensional Composite Piezo-Silicon Resonant Cavities,” 2019 Joint Conference of the IEEE International Frequency Control Symposium and European Frequency and Time Forum (EFTF/IFC), 2019, pp. 1-3.

[12] H. Mansoorzare and R. Abdolvand, “Acoustoelectric Non-Reciprocity in Lithium Niobate-on-Silicon Delay Lines,” in IEEE Electron Device Letters, vol. 41, no. 9, pp. 1444-1447, Sept. 2020.

[13] H. Mansoorzare and R. Abdolvand, “A Thin-Film Piezo-Silicon Acoustoelectric Isolator with More than 30 dB Non-Reciprocal Transmission,” 2021 IEEE 34th International Conference on Micro Electro Mechanical Systems (MEMS), 2021, pp. 470-473.

[14] L. Solie. “Tapered transducers - design and applications.” 1998 IEEE Ultrasonics Symposium. Proceedings (Cat. No. 98CH36102). Vol. 1. IEEE, 1998.

[15] G. Martin and B. Steiner, “SAW filters including one-focus slanted finger interdigital transducers,” 2001 IEEE Ultrasonics Symposium. Proceedings. An International Symposium (Cat. No.01CH37263), 2001, pp. 45-48 vol.1.

CONTACT

*H. Mansoorzare, tel: +1-352-3464400;
Hakha@knights.ucf.edu